HHS Public Access

Author manuscript

J Immunol. Author manuscript; available in PMC 2017 October 01.

Published in final edited form as:

J Immunol. 2016 October 01; 197(7): 2686–2694. doi:10.4049/jimmunol.1501162.

Nestin-Expressing Precursors Give Rise to Both Endothelial as well as Nonendothelial Lymph Node Stromal Cells

Jasper J. Koning[*], **Tanja Konijn**[*], **Kim A. Lakeman**[*], **Tom O'Toole**[*], **Keane J. G. Kenswil**[†,‡], **Marc H. G. P. Raaijmakers**[†,‡], **Tatyana V. Michurina**[§,¶,‖,#], **Grigori Enikolopov**[§,¶,‖,#], and **Reina E. Mebius**[*]

[*]Department of Molecular Cell Biology and Immunology, VU University Medical Center, 1081 HZ Amsterdam, the Netherlands [†]Department of Hematology, Erasmus University Medical Center, 3015 GE Rotterdam, the Netherlands [‡]Erasmus Stem Cell Institute, Erasmus University Medical Center, 3015 GE Rotterdam, the Netherlands [§]Department of Anesthesiology, Stony Brook University, Stony Brook, NY 11794 [¶]Center for Developmental Genetics, Stony Brook University, Stony Brook, NY 11794 [‖]Cold Spring Harbor Laboratory, Cold Spring Harbor, New York, NY 11724 [#]Department of Nano-, Bio-, Information, and Cognitive Sciences, Moscow Institute of Physics and Technology, 123182 Moscow, Russia

Abstract

During embryogenesis, lymph nodes form through intimate interaction between lymphoid tissue inducer and lymphoid tissue organizer (LTo) cells. Shortly after birth in mice, specialized stromal cell subsets arise that organize microenvironments within the lymph nodes; however, their direct precursors have not yet been identified. In the bone marrow, mesenchymal stem cells are labeled with GFP in nestin-GFP mice, and we show that during all stages of development, nestin$^+$ cells are present within lymph nodes of these mice. At day of birth, both mesenchymal CD31$^-$ and endothelial CD31$^+$ LTo cells were GFP$^+$, and only the population of CD31$^-$ LTo cells contained mesenchymal precursors. These CD31$^-$nestin$^+$ cells are found in the T and B cell zones or in close association with high endothelial venules in adult lymph nodes. Fate mapping of nestin$^+$ cells unambiguously revealed the contribution of nestin$^+$ precursor cells to the mesenchymal as well as the endothelial stromal populations within lymph nodes. However, postnatal tamoxifen induced targeting of nestin$^+$ cells in nes-creER mice showed that most endothelial cells and only a minority of the nonendothelial cells were labeled. Overall our data show that nestin$^+$ cells contribute to all subsets of the complex stromal populations that can be found in lymph nodes.

Lymph nodes are situated such that incoming Ags are efficiently presented to immune cells, allowing rapid responses to infectious agents. Their formation starts during embryogenesis with the attraction of lymphoid tissue inducer (LTi) cells, which are of hematopoietic origin

Address correspondence and reprint requests to Prof. Reina E. Mebius, Department of Molecular Cell Biology and Immunology, VU University Medical Center, Van der Boechorststraat 7, 1081 HZ Amsterdam, the Netherlands. r.mebius@vumc.nl.

ORCIDs: 0000-0003-2243-4857 (J.J.K.); 0000-0002-8612-4367 (T.V.M.); 0000-0001-8178-8917 (G.E.); 0000-0003-0451-7464 (R.E.M.).

Disclosures

The authors have no financial conflicts of interest.

and part of the family of innate lymphoid cells, to the presumptive lymph node site (1, 2). This attraction is initiated through the expression of CXCL13 by mesenchymal precursors (3). Accumulating LTi cells start to express lymphotoxin $\alpha_1\beta_2$ that allows signaling through lymphotoxin β receptor, which is expressed by mesenchymal precursor cells. These cells then differentiate into lymphoid tissue organizer (LTo) cells and start to produce chemokines, cytokines, and adhesion molecules that result in the attraction, survival, and retention of more LTi cells, leading to a lymph node anlage (4–6). Eventually, LTo cells give rise to the various lymph node stromal subsets. Endothelial cells also play an important role in the formation of lymph nodes because ablation of lymphotoxin β receptor expression on endothelial cells affects peripheral lymph node development (7).

Shortly after birth, when lymph nodes are being populated with lymphocytes, lymph nodes increase in size while microdomains for T and B cells are being established by various stromal populations (8–13).

The lymph node stromal compartment is formed by several cell types of endothelial and mesenchymal origin, which serve crucial functions for proper immune responses. So is the entry of naive lymphocytes from the bloodstream crucially controlled by specialized blood endothelial cells (BECs), which form the high endothelial venules (HEVs). Whereas the entry of Ag, either freely floating in lymph fluid or captured by APCs, is dependent on functional lymphatic vessels, which are formed by lymphatic endothelial cells (LECs).

The stromal cells of mesenchymal origin can be divided into cells that reside in the T cell area, the fibroblastic reticular cells (FRCs); cells that are present in the B cell area, the follicular dendritic cells (FDCs); and cells that associate with the subcapsular sinus, the marginal reticular cells (MRCs) (14–16).

The FRC subset has been shown to not only provide a structural backbone for the migration of T cells searching for their cognate Ag, but they are in fact actively guiding T cells while providing them with survival signals (8, 14, 17). Furthermore, they regulate the pool of activated T cells (18), have the ability to present peripheral tissue Ags to induce Ag-specific T cell tolerance (19), maintain regulatory T cells (20), and can induce tissue-specific homing molecules on T cells (21, 22).

For the spleen, it was shown that all mesenchymal stromal subsets share a common precursor (23), although the direct precursors for the different mesenchymal-derived stromal subsets in lymph nodes have not been identified yet. The expression of the mesenchymal lineage markers platelet-derived growth factor receptor (PDGFR)-α and PDGFR-β on LTo cells suggests that they also may be of mesenchymal origin (4, 17, 24). Therefore, mesenchymal stem cells serve as good precursor candidates. The discovery that mesenchymal stem cells in the bone marrow are confined to a population of cells that are marked by transgenic expression of nestin (25) led us to investigate the contribution of nestin-expressing precursors to the lymph node stromal cell compartment. Using various nestin-transgenic mice, we show that nestin labels different types of mesenchymal and endothelial precursors that are present in primitive lymph nodes during the early stages of development and remained present during definitive organ formation. Embryonic-induced

lineage tracing showed that nestin-expressing precursors gave rise to both mesenchymal- as well as endothelial-derived mature stromal cells whereas postnatal-induced lineage tracing mainly targeted endothelial cells.

Materials and Methods

Mice

C57BL/6 mice were bred at our own facility and maintained under standard animal housing conditions. The nestin-GFP mouse line was generated as described (26). B6.Cg-Tg(Nestin-cre)1Kln/J (nestin-cre) and B6;129-*Gt(ROSA)26Sor*^{tm2Sho}/J (ROSA26-lsl-GFP) strains were obtained from The Jackson Laboratory. Nestin-Cre^{ERT2} mice (27) were crossed with *RCE:loxP* mice (28). All animal experiments were approved by local Ethics Committee regulations.

Single-cell suspension

For fibroblastic CFU (CFU-F) assays, isolated peripheral lymph nodes (which include inguinal, brachial, and axillary lymph nodes) and mesenteric lymph nodes were cleared from surrounding fat/tissue and subsequently cut into small pieces followed by enzymatic digestion in DMEM containing Blendzyme 2 (150 μg/ml), DNase I (200 μg/ml; both Roche Applied Sciences, Almere, the Netherlands), 2% FCS, and 2% antibiotics (digestion medium) for 15 min, 37°C while continuously stirring. Remaining fragments were further digested for another 15 min, 37°C. For FACS analysis, lymph node singlecell suspensions were made according to the protocol described by Fletcher et al. (29). In short, isolated peripheral lymph nodes (which include axillary, brachial, inguinal, and popliteal lymph nodes) and mesenteric lymph nodes were pierced with a 25-gauge needle and placed in RPMI 1640 on ice. Upon the start of digestion, lymph nodes were transferred to a tube containing 2 ml of freshly prepared digestion medium (RPMI 1640) containing 0.8 mg/ml Dispase II, 0.2 mg/ml collagenase P, and 0.1 mg/ml DNase I (all from Roche). Tubes were incubated at 37°C for 20 min and gently vortexed every 5 min. After 20 min, suspensions were gently pipetted to break the lymph node capsule. Upon settlement of large fragments, supernatant was transferred to a collection tube containing 10 ml of ice-cold FACS buffer (2% FCS, 5 mM EDTA in PBS) and centrifuged (5 min, 300 × *g*, 4°C). Two microliters of digestion medium was added to the digestion tube and incubated at 37°C while regularly mixing. After 10 min, digestion medium was robustly mixed with 1 ml by pipette. Upon settlement of large fragments, medium with cells was transferred to a previous collection tube with new FACS buffer and centrifuged (5 min, 300 × *g*, 4°C). Again, 2 ml of digestion medium was added to the digestion tube and mixture was robustly mixed every 5 min until all remaining fragments were digested.

Flow cytometry

Data were acquired on a CyAn ADP high-performance research flow cytometer (Beckman Coulter) and were analyzed with Summit software v4.3. Single-stained cells were used to compensate for spectral overlap. Fluorescence minus one–stained cells were used to set boundaries between positive and negative cells. 7-Aminoactinomycin D or Sytox Blue (Molecular Probes) staining was used to exclude dead cells. Cell sorting was performed on a

MoFlo high-speed cell sorter (Dako Cytomation, Glostrup, Denmark) equipped with Summit software. Sorted cells were collected in appropriate culture medium and further analyzed using in vitro cultures.

CFU-F assays

For CFU-F assays, cells were seeded in at least two different concentrations in 2 ml of MesenCult plus stimulatory supplements (Stemcell Technologies, Lyon, France) and 2% antibiotics per well in a six-wells plate. CFU-F assays were always performed in duplicate. After 2 wk of culture, cells were washed twice with PBS, fixed in methanol, and stained with Giemsa. CFU-F were counted using a stereo microscope. Cell clusters containing ≥10 cells were considered as a colony. Absolute numbers of CFU-F were calculated as follows: the frequency of CFU-F per million seeded cells was determined, and this CFU-F frequency per million cells was subsequently adapted for the total amount of lymph node cells derived from a set of peripheral lymph nodes (inguinal, brachial, and axillary) or mesenteric lymph nodes.

In vitro differentiation assay

Adipocyte differentiation was induced by culturing cells in DMEM supplemented with 10% FCS, 1% antibiotics, 100 nM dexamethasone (Sigma-Aldrich, Zwijndrecht, the Netherlands), 0.1 mM indomethacin, 0.5 mM 3-isobutyl-1-methylzanthine (Sigma-Aldrich), and 5 μg/ml insulin (Sigma-Aldrich). Osteogenic differentiation was induced in DMEM supplemented with 10% FCS, 1% antibiotics, 0.1 μM dexamethasone, 10 mM β-glycerophosphate (Sigma-Aldrich), and 25 μg/ml L-ascorbic acid 2-phosphate (Sigma-Aldrich). Medium was replaced two times per week for a period of 4 wk.

To determine transcript upregulation, cells were lysed, after which mRNA was isolated from total RNA using an mRNA capture kit (Roche) and cDNA was synthesized using a reverse transcriptase kit (Promega Benelux, Leiden, the Netherlands) according to the manufacturers' protocols. RT-PCR was performed on an ABI Prism 7900HT sequence detection system (PE Applied Biosystems). Total volume of the reaction mixture was 10 μl, containing cDNA, 300 nM of each primer, and SYBR Green master mix (PE Applied Biosystems). From a set of eight housekeeping genes, the two most stable were selected. The comparative cycle threshold method (ΔCt) was used to indicate relative changes in mRNA levels between samples. Relative mRNA levels of unstimulated cells were set at 1 for each time point. Primer sequences are listed in Table I.

Immunofluorescence microscopy

Nestin-GFP$^+$ embryos of 14.5 d after conception were fixed for 30 min in paraformaldehyde in PBS, cryoprotected overnight in sucrose (30% [w/v] in PBS), and subsequently embedded in OCT compound (Sakura Finetek Europe) and stored at −80°C until sectioning. Lymph nodes from nestin-GFP, nestin-cre/ROSA26-GFP, and nestin-creER/ROSA26-GFP mice were fixed in paraformaldehyde in PBS for 10 min, cryoprotected, and subsequently embedded in OCT compound. For identification of primordial lymph nodes, embryos were serially sectioned (8 mm) on gelatin-coated slides, and every 10th slide was stained with anti-CD4 and anti-MAdCAM-1. Immunofluorescence staining was performed in PBS,

supplemented with 0.1% (w/v) BSA or Earle's balanced salt solution in the case of TRANCE staining. Biotinylated anti-TRANCE (IK22/5; eBioscience) was visualized with a tyramide signal amplification kit plus HRP-streptavidin and Alexa Fluor 546-tyramide (Invitrogen). Sections were enclosed in Vinol (Air Products and Chemicals, Allentown, PA) supplemented with DAPI (Invitrogen) and analyzed on a Leica DM6000 fluorescence microscope or a Leica TCS-SP2-AOBS confocal laser scanning microscope (both from Leica Microsystems), and images were obtained with Leica software.

Abs

The following Abs were used in variable combinations for flow cytometry or immunofluorescence: unconjugated anti-CD31 (ERMP12, provided by P. Leenen, Erasmus University Rotterdam, Rotterdam, the Netherlands), anti-gp38 (anti-podoplanin, clone 8.1.1, obtained from the Developmental Studies Hybridoma Bank at the University of Iowa, Iowa City, IA), anti-VEGFR2 and anti–Lyve-1 (Millipore), TUJ-1 (Ab to neuron-specific βIII-tubulin, ab18207; Abcam), anti-GFP (Invitrogen), anti-desmin (BD Biosciences, Breda, the Netherlands), anti–α smooth muscle actin (α-SMA; clone 1A4; Sigma-Aldrich), anti-NG2 (Chemicon International, Millipore), MECA79 (anti-PNAd); biotinylated anti-CD35 (8C12), FITC-labeled anti–ICAM-1 (CD54), and anti–VCAM-1 (CD106); PE-labeled anti–ICAM-1; PE-Cy7–labeled anti-CD45 (clone 30F11); Alexa Fluor 555–labeled anti-CD4 (clone GK1.5); allophycocyanin anti–VCAM-1; Alexa Fluor 647–labeled anti-CD45 (clone MP33); and anti-MAdCAM-1 (MECA-367). Clones GK1.5, MP33, and MECA-367 were affinity purified from hybridoma cell culture supernatants with protein G–Sepharose (Pharmacia, Uppsala, Sweden) and subsequently labeled with Alexa Fluor 555 (GK1.5) or Alexa Fluor 647 (MP33 and MECA-367) (Invitrogen). Unconjugated Abs were detected with species-specific secondary reagents, namely goat anti-rat Alexa Fluor 488 or 647, goat anti-rabbit Alexa Fluor 488 or 647, and goat anti-hamster Alexa Fluor 488 or 647 (all Invitrogen). Unless indicated otherwise, all Abs were obtained from eBioscience (San Diego, CA).

Results

Nestin-expressing cells are present during initiation of lymph node development

We started off by assessing the presence of nestin$^+$ cells in early presumptive lymph nodes of embryonic day (E)14.5 embryo's from mice that express GFP under control of the promoter and the nervous system-specific enhancer present in the second intron of the rat nestin gene (nestin-GFP mice) (26). Early lymph node structures can be identified by the combined analysis of CD4 expressed on LTi cells and MAdCAM-1 on stromal cells (3, 5, 30, 31). Analysis of E14.5 nestin-GFP embryos revealed normal clusters of LTi cells together with MAdCAM-1$^+$ cells (Fig. 1A, 1B). All clusters that we could identify at this stage, which are cervical lymph node, facial lymph node, axillary lymph node, and brachial lymph node anlagen, developed in the vicinity of bright GFP-expressing structures that uniformly coexpressed the neuron-specific marker βIII-tubulin, and therefore resembled nerve bundles (Fig. 1C). Within LTi clusters, we observed cells that expressed GFP and MAdCAM-1 but lacked βIII-tubulin expression (Fig. 1A–C). Most of these nonneuronal nestin$^+$ cells expressed endothelial markers CD31 and VEGFR2, whereas we also observed

nestin^{+} cells that were CD31^{-} or VEGFR2^{-} that were found closely associated to nestin^{+}CD31^{+} cells (Fig. 1D, 1E). These data indicate the presence of different nestin^{+} populations in developing lymph nodes.

Nestin expression marks lymphoid tissue organizer cells

During subsequent stages of embryonic lymph node development, mesenchymal stromal precursor cells continue to differentiate into LTo cells upon lymphotoxin-mediated signaling provided by LTi cells. This results in the additional induction of chemokines (CXCL13, CCL21, CCL19), adhesion molecules (ICAM-1, VCAM-1), as well as TRANCE and IL-7 (5, 24, 30) needed for the attraction, retention, and survival of lymphocytes. Additionally, endothelial cells have also been described to contain lymphotoxin-dependent organizer capacity (7). At day of birth, LTo cells are abundantly present within lymph nodes, and the expression of VCAM-1 and ICAM-1 marks different LTo stromal populations, including endothelial cells (30).

GFP expression analysis at day of birth showed that nearly all ICAM-1/VCAM-1-expressing cells (IV^{int} and IV^{high}) were nestin^{+}, whereas only a small fraction of IV^{-} cells expressed GFP. I^{high}V$^{-/int}$ cells were also found to uniformly express nestin (Fig. 2A–C).

Within adult lymph nodes, the various stromal subsets can be identified by combined expression for podoplanin (gp38) and CD31 (17). Analysis of lymph node stromal cells at day of birth revealed that all IV^{int} and IV^{high} cells expressed gp38, whereas endothelial markers CD31 and VEGFR2 were restricted to the I^{high}V$^{-/int}$ population (Fig. 2D, 2E). Taken together, these data identify nestin expression in two populations of early stromal constituents, namely the gp38-expressing IV^{int} and IV^{high} subset and the CD31-expressing I^{high}V$^{-/int}$ population, that have important organizer capacity in developing lymph nodes.

In the bone marrow, nesGFP cells were found to contain mesenchymal activity and clonogenicity (25). Upon sorting the different stromal populations out of lymph nodes at day of birth, we found that both IV^{-} and I^{high}V$^{-/int}$ were not able to form colonies but that the colony-forming capacity was restricted to the subsets defined as nonendothelial CD31^{-} LTo cells (IV^{int}, IV^{high}, Fig. 2F). Surprisingly, at this time point, these cells did not have the capacity to differentiate into adipocytes or osteocytes under the appropriate culture conditions (Fig. 2I).

To determine when mesenchymal precursors were most abundantly present within developing lymph nodes, we performed CFU-F assays at several time points after birth. The highest levels of absolute numbers of CFU-F were found at week 2 of age whereas substantial numbers of CFU-F could still be measured at 8 wk of age (Fig. 2G). At this stage, these cells were now able to differentiate into adipocytes and showed differential upregulation of osteogenic genes (Fig. 2I). Although absolute numbers of mesenchymal precursors are highest at 2 wk of age, the absolute number of stromal cells (CD45^{-}) started to increase only after week 2 (Fig. 2H).

Postnatal nestin expression decreases over time and remains present in adult lymph nodes

We analyzed the presence of nesGFP cells during postnatal lymph node development as well and observed a decrease in the absolute number of nesGFP$^+$ cells after week 3 (Fig. 3A, 3B). Additional analysis using gp38 and CD31 (Fig. 3C) revealed that nestin$^+$ cells can be found in all subsets but mainly are FRCs (Fig. 3A, 3B). Despite the decrease in absolute number of nestin$^+$ cells in adult mice we still observed substantial GFP expression in both the nonendothelial stromal cells (CD45$^-$gp38$^+$CD31$^-$) as well as in BECs (CD45$^-$gp38$^-$CD31$^+$) (Fig. 3A, 3B). Within the LEC population (CD45$^-$gp38$^+$CD31$^+$) we did not observe nestin$^+$ cells in adult mice; however, we observed low numbers of GFP-expressing cells within the double-negative (DN) population (CD45$^-$gp38$^-$CD31$^-$, Fig. 3A, 3B). Based on GFP expression levels together with gp38, we were able to distinguish three populations (Fig. 3D). Interestingly, the DN population in adult mice almost completely consisted of GFP^{high}-expressing cells (Fig. 3E). Within the gp38$^+$CD31$^-$ population most cells were GFP^{dim} although we also observed GFP^{high} cells (Fig. 3E).

Using immunofluorescence we observed nestin$^+$ cells within the T cell area, the B cell area, as well as the subcapsular sinus (Fig. 3G–J). Within the T cell area, nonendothelial nestin$^+$ cells expressed gp38 (Fig. 3H) as well as desmin and α-SMA (Fig. 3K) and were regularly found in close association with HEVs (Fig. 3L). Recently, splenic FDC precursors were described as perivascular cells that expressed PDGFR-β and NG2 (32). In lymph nodes, we could also identify perivascular nestin$^+$ cells that expressed PDGFR-β (Fig. 3M) but not NG2 (data not shown).

The nestin$^+$ cells that localized around HEVs are CD31$^-$ but do express α-SMA and desmin, known markers for FRCs as well as pericytes (17). Nestin$^+$ cells that expressed CD31 could be found within the T cell area and the B cell area as part of what appeared to be small capillaries (Fig. 3L and data not shown). In the subcapsular sinus, nestin$^+$ cells occasionally expressed TRANCE, although never in combination with MAdCAM-1 (Fig. 3J), indicating that nestin$^+$ cells were distinct from MRCs (15). Within the adult lymph nodes, nestin$^+$ cells never expressed β-tubulin (data not shown).

Nestin precursors give rise to the major subsets of mesenchymal-and endothelial-derived lymph node stromal cells

Our data show that nestin$^+$ cells include mesenchymal and endothelial cells that are present during all stages of lymph node development, potentially acting as precursors for the different stromal subsets present within lymph nodes. To assess their contribution to lymph node stromal cell populations, we crossed mice expressing Cre recombinase under the control of a minimal promotor and a 1.8-kb nestin second intron enhancer (nesCRE) together with a ROSA-GFP reporter. This allowed lineage tracing of all cells that expressed the nestin-cre transgene (25, 33).

FACS analysis of lymph node single-cell suspensions showed that most FRCs (gp38$^+$CD31$^-$) were derived from nestin$^+$ precursors (Fig. 4A, 4B, 4D). We hardly observed GFP expression in the DN subset (gp38$^-$CD31$^-$, Fig. 4B). Upon immunofluorescence

staining we confirmed that podoplanin-expressing FRCs were GFP$^+$ (Fig. 4C, 4E), that FDCs within the B cell area expressed GFP (Fig. 4F), and that TRANCE$^+$MAdCAM-1$^+$ MRCs within the subcapsular sinus were expressing GFP (Fig. 4G).

Additionally, most endothelial cells (CD45$^-$gp38$^-$CD31$^+$) were labeled with GFP (Fig. 4A, 4B, 4H). Immunofluorescence analysis showed that capillary vasculature structures as well as HEVs were GFP$^+$ in both peripheral lymph nodes and mesenteric lymph nodes (Fig. 4I). Furthermore, also LECs (gp38$^+$CD31$^+$) expressed GFP, both by FACS as well as immunofluorescence analysis, suggesting that most LECs present within lymph nodes were also derived from nestin-expressing precursors (Fig. 4A, 4B, 4I–K).

Overall, these results indicate that nestin-cre marks cells that belong to the endothelial as well as the mesenchymal stromal subsets.

During later stages of lymph node development, nestin predominantly labels endothelial cells

To more specifically identify the contribution of nestin$^+$ cells to the lymph node stromal compartment after birth, we used mice that expressed an inducible Cre recombinase under the minimal nestin-promoter and second intron enhancer (nes-creER) (27) together with a ROSA26-GFP reporter. Mice received tamoxifen at day 17 after birth (p17) and were analyzed 4 wk later.

At the time of tamoxifen administration, lymph nodes from nestin-GFP mice harbored abundant numbers of nestin$^+$ cells (Fig. 3A, 3B). Surprisingly, tamoxifen administration to nescreER mice at p17 resulted in GFP labeling of only a minor fraction of stromal cells in both peripheral as well as mesenteric lymph nodes and mainly labeled BECs and LECs (Fig. 5A, 5B). The amount of GFP-labeled FRCs or DN cells in peripheral lymph nodes was undetectable by FACS analysis whereas in mesenteric lymph nodes only few cells were labeled (Fig. 5A, 5B).

Histological analysis revealed that HEVs were predominantly labeled in a mosaic pattern (Fig. 5C); additionally, GFP-expressing capillary endothelial cells as well as lymphatic endothelial cells were found (Fig. 5D, 5G). The few labeled nonendothelial gp38$^+$ cells appeared as single cells (Fig. 5E, 5F). These data show that during postnatal lymph node development, nestin-cre predominantly marks endothelial cells.

Discussion

Lymph node stromal cells comprise a heterogeneous population of both endothelial as well as nonendothelial stromal cells that play important roles in immunity. The embryonic origin of nonendothelial stromal cells in lymph nodes is as of today still unknown. It was shown before that nestin labels a subset of nonneuronal precursor cells in the adult bone marrow that showed mesenchymal stem cell properties as well as important functions for hematopoietic stem cell maintenance (25). Similar to the bone marrow, lymph node stromal cells support progeny of hematopoietic cells and additionally control immune responses in various ways (34, 35). By using different nestin transgenic mice, we show in the present

study that the progeny of nestin$^+$ cells make up most stromal cells within lymph nodes, not only mesenchymal stromal cells but also endothelial cells. Within adult lymph node, two subsets of nestin$^+$ cells were distinguished, namely mesenchymal gp38$^+$nestin$^+$ cells and endothelial CD31$^+$nestin$^+$ cells. The gp38$^+$ nestin$^+$ cells were found within the reticular network of the T and B cell area or around HEVs. A similar distribution has been described for precursor cells that give rise to FRCs (36). The CD31$^+$ nestin$^+$ cells were found within the T cell and B cell area as single cells within capillaries.

Using transgenic mice that express GFP under the control of the nestin promotor and second intron enhancer (25, 26) we showed that mesenchymal and endothelial stromal cells were marked with GFP in lymph node anlagen during early fetal lymph node formation. Later on, shortly after birth, all cells that have been described to contain lymph tissue organizer capacity, endothelial and nonendothelial cells (7, 24, 30), were marked with GFP. We have described that LTo cells give rise to the lymph node stromal compartment (37), and our data indicated that stromal cells are derived from nestin-expressing precursors. Indeed, in mice that carried a nestin-cre construct together with a ROSA26-GFP reporter that allowed genetic lineage tracing, we showed that most stromal cells were derived from cells that once expressed nestin. Although most stromal cells are labeled with GFP, we also observed GFP$^-$ stromal cells in all populations, indicating that other precursor cells can contribute to endothelial and mesenchymal stromal subsets as well, especially the DN population because only a minor proportion of these cells was marked with GFP upon lineage tracing.

DN cells have been proposed to be precursors of FRCs (36). Our data with nes-cre × ROSA-GFP mice show that a small proportion of DN cells are labeled as well. Furthermore, our nes-GFP data show that at day of birth, also a proportion of DN cells are nestin$^+$ (Fig. 2B, 2C), and nes-GFP mice analyzed at 2, 3, and 6 wk after birth show that a proportion of DN cells is still nestin$^+$ (Fig. 3E, 3F). Interestingly, the nestin$^+$ DN stromal cells are almost exclusively nestin-GFP^{high} cells whereas most FRCs are GFP^{dim} and only a small proportion of FRCs are GFP^{high}. This leaves the possibility for a model in which a proportion of CD31$^-$gp38$^-$GFP^{high} cells differentiate into CD31$^-$gp38$^+$GFP^{high} cells that gradually loose GFP expression upon further maturation, hence gp38$^+$GFP^{dim} cells, that ultimately lose GFP expression upon final maturation in adult lymph nodes.

Postnatal induction of lineage tracing of nestin$^+$ cells at p17 using the nes-creER construct mainly targeted endothelial cells, including high endothelial venules, capillaries, and lymphatic endothelial cells. Although in nes-GFP mice at p17 a substantial amount of mesenchymal stromal cells was marked with GFP, we observed only very few mesenchymal-derived cells that were marked upon postnatal lineage tracing induction at p17 in nes-creER mice. Although this could be due to the different constructs that were used to mark the nestin-expressing cells, our data may also highlight different developmental kinetics between the endothelial and nonendothelial stromal subpopulations. Because we were able to mark few nonendothelial stromal cells in nes-creER mice after induction of lineage tracing at p17, the tamoxifen induction may have come after the moment that most nestin-expressing precursors differentiated into the different mesenchymal stromal cell subsets. The decrease of mesenchymal precursors after p14, as measured by the FU-F assay, further supports this model. Unfortunately, we were not able to successfully induce lineage

tracing shortly after birth (at day 4 after birth), as early tamoxifen administration was not compatible with life.

Altogether, distinct populations of lymph node stromal cells make up the various niches in which immune cells reside and on which they depend for their function. In this study, we show that most of these cell types during embryonic and postnatal lymph node development are nestin^{+}. Similar findings have been described for the bone marrow (38, 39) indicating that nestin^{+} cells are not only important cellular components for the hematopoietic stem cell niche but also generate the niche in which their progeny reside.

Acknowledgments

We thank S. A. van de Pavert and G. Kraal for carefully reading the manuscript.

This work was supported by Netherlands Earth and Life Sciences Foundation Grant 820.02.004 (to J.J.K.), Netherlands Organization for Scientific Research Vici Grant 918.56.612 (to R.E.M.), and by National Institute of Aging Grant R01AG040209, New York State Stem Cell Science Grant C029569, and Russian Ministry of Education and Science Grant 11.G34.31.0071 (to G.E.).

Abbreviations

BEC	blood endothelial cell
CFU-F	fibroblastic CFU
DN	double-negative
E	embryonic day
FDC	follicular dendritic cell
FRC	fibroblastic reticular cell
HEV	high endothelial venule
LEC	lymphatic endothelial cell
LTi	lymphoid tissue inducer
LTo	lymphoid tissue organizer
MRC	marginal reticular cell
nestin-cre	B6.Cg-Tg(Nestin-cre)1Kln/J
p17	day 17 after birth
PDGFR	platelet-derived growth factor receptor
ROSA26-GFP	B6; 129-*Gt(ROSA)26Sor*^{tm2Sho}/J
α-SMA	α smooth muscle actin

References

1. Spits H, Di Santo JP. The expanding family of innate lymphoid cells: regulators and effectors of immunity and tissue remodeling. Nat Immunol. 2011; 12:21–27. [PubMed: 21113163]
2. van de Pavert SA, Mebius RE. New insights into the development of lymphoid tissues. Nat Rev Immunol. 2010; 10:664–674. [PubMed: 20706277]
3. van de Pavert SA, Olivier BJ, Goverse G, Vondenhoff MF, Greuter M, Beke P, Kusser K, Höpken UE, Lipp M, Niederreither K, et al. Chemokine CXCL13 is essential for lymph node initiation and is induced by retinoic acid and neuronal stimulation. Nat Immunol. 2009; 10:1193–1199. [PubMed: 19783990]
4. Honda K, Nakano H, Yoshida H, Nishikawa S, Rennert P, Ikuta K, Tamechika M, Yamaguchi K, Fukumoto T, Chiba T, Nishikawa SI. Molecular basis for hematopoietic/mesenchymal interaction during initiation of Peyer's patch organogenesis. J Exp Med. 2001; 193:621–630. [PubMed: 11238592]
5. Vondenhoff MF, Greuter M, Goverse G, Elewaut D, Dewint P, Ware CF, Hoorweg K, Kraal G, Mebius RE. LTβR signaling induces cytokine expression and up-regulates lymphangiogenic factors in lymph node anlagen. J Immunol. 2009; 182:5439–5445. [PubMed: 19380791]
6. Yoshida H, Naito A, Inoue J, Satoh M, Santee-Cooper SM, Ware CF, Togawa A, Nishikawa S, Nishikawa S. Different cytokines induce surface lymphotoxin-αβ on IL-7 receptor-α cells that differentially engender lymph nodes and Peyer's patches. Immunity. 2002; 17:823–833. [PubMed: 12479827]
7. Onder L, Danuser R, Scandella E, Firner S, Chai Q, Hehlgans T, Stein JV, Ludewig B. Endothelial cell-specific lymphotoxin-β receptor signaling is critical for lymph node and high endothelial venule formation. J Exp Med. 2013; 210:465–473. [PubMed: 23420877]
8. Bajénoff M, Glaichenhaus N, Germain RN. Fibroblastic reticular cells guide T lymphocyte entry into and migration within the splenic T cell zone. J Immunol. 2008; 181:3947–3954. [PubMed: 18768849]
9. Cupedo T, Lund FE, Ngo VN, Randall TD, Jansen W, Greuter MJ, de Waal-Malefyt R, Kraal G, Cyster JG, Mebius RE. Initiation of cellular organization in lymph nodes is regulated by non-B cell-derived signals and is not dependent on CXC chemokine ligand 13. J Immunol. 2004; 173:4889–4896. [PubMed: 15470030]
10. Fasnacht N, Huang HY, Koch U, Favre S, Auderset F, Chai Q, Onder L, Kallert S, Pinschewer DD, MacDonald HR, et al. Specific fibroblastic niches in secondary lymphoid organs orchestrate distinct Notch-regulated immune responses. J Exp Med. 2014; 211:2265–2279. [PubMed: 25311507]
11. Förster R, Mattis AE, Kremmer E, Wolf E, Brem G, Lipp M. A putative chemokine receptor, BLR1, directs B cell migration to defined lymphoid organs and specific anatomic compartments of the spleen. Cell. 1996; 87:1037–1047. [PubMed: 8978608]
12. Förster R, Schubel A, Breitfeld D, Kremmer E, Renner-Müller I, Wolf E, Lipp M. CCR7 coordinates the primary immune response by establishing functional microenvironments in secondary lymphoid organs. Cell. 1999; 99:23–33. [PubMed: 10520991]
13. Gunn MD, Tangemann K, Tam C, Cyster JG, Rosen SD, Williams LT. A chemokine expressed in lymphoid high endothelial venules promotes the adhesion and chemotaxis of naive T lymphocytes. Proc Natl Acad Sci USA. 1998; 95:258–263. [PubMed: 9419363]
14. Bajénoff M, Egen JG, Koo LY, Laugier JP, Brau F, Glaichenhaus N, Germain RN. Stromal cell networks regulate lymphocyte entry, migration, and territoriality in lymph nodes. Immunity. 2006; 25:989–1001. [PubMed: 17112751]
15. Katakai T, Suto H, Sugai M, Gonda H, Togawa A, Suematsu S, Ebisuno Y, Katagiri K, Kinashi T, Shimizu A. Organizer-like reticular stromal cell layer common to adult secondary lymphoid organs. J Immunol. 2008; 181:6189–6200. [PubMed: 18941209]
16. Mueller SN, Germain RN. Stromal cell contributions to the homeostasis and functionality of the immune system. Nat Rev Immunol. 2009; 9:618–629. [PubMed: 19644499]

17. Link A, Vogt TK, Favre S, Britschgi MR, Acha-Orbea H, Hinz B, Cyster JG, Luther SA. Fibroblastic reticular cells in lymph nodes regulate the homeostasis of naive T cells. Nat Immunol. 2007; 8:1255–1265. [PubMed: 17893676]
18. Lukacs-Kornek V, Malhotra D, Fletcher AL, Acton SE, Elpek KG, Tayalia P, Collier AR, Turley SJ. Regulated release of nitric oxide by nonhematopoietic stroma controls expansion of the activated T cell pool in lymph nodes. Nat Immunol. 2011; 12:1096–1104. [PubMed: 21926986]
19. Fletcher AL, Malhotra D, Turley SJ. Lymph node stroma broaden the peripheral tolerance paradigm. Trends Immunol. 2011; 32:12–18. [PubMed: 21147035]
20. Baptista AP, Roozendaal R, Reijmers RM, Koning JJ, Unger WW, Greuter M, Keuning ED, Molenaar R, Goverse G, Sneeboer MM, et al. Lymph node stromal cells constrain immunity via MHC class II selfantigen presentation. eLife. 2014; 3:e04433.
21. Hammerschmidt SI, Ahrendt M, Bode U, Wahl B, Kremmer E, Förster R, Pabst O. Stromal mesenteric lymph node cells are essential for the generation of gut-homing T cells in vivo. J Exp Med. 2008; 205:2483–2490. [PubMed: 18852290]
22. Molenaar R, Greuter M, van der Marel AP, Roozendaal R, Martin SF, Edele F, Huehn J, Förster R, O'Toole T, Jansen W, et al. Lymph node stromal cells support dendritic cell-induced gut-homing of T cells. J Immunol. 2009; 183:6395–6402. [PubMed: 19841174]
23. Castagnaro L, Lenti E, Maruzzelli S, Spinardi L, Migliori E, Farinello D, Sitia G, Harrelson Z, Evans SM, Guidotti LG, et al. Nkx2-5^{+}islet1^{+} mesenchymal precursors generate distinct spleen stromal cell subsets and participate in restoring stromal network integrity. Immunity. 2013; 38:782–791. [PubMed: 23601687]
24. Bénézech C, White A, Mader E, Serre K, Parnell S, Pfeffer K, Ware CF, Anderson G, Caamaño JH. Ontogeny of stromal organizer cells during lymph node development. J Immunol. 2010; 184:4521–4530. [PubMed: 20237296]
25. Mendez-Ferrer S, Michurina TV, Ferraro F, Mazloom AR, Macarthur BD, Lira SA, Scadden DT, Ma'ayan A, Enikolopov GN, Frenette PS. Mesenchymal and haematopoietic stem cells form a unique bone marrow niche. Nature. 2010; 466:829–834. [PubMed: 20703299]
26. Mignone JL, Kukekov V, Chiang AS, Steindler D, Enikolopov G. Neural stem and progenitor cells in nestin-GFP transgenic mice. J Comp Neurol. 2004; 469:311–324. [PubMed: 14730584]
27. Balordi F, Fishell G. Mosaic removal of hedgehog signaling in the adult SVZ reveals that the residual wild-type stem cells have a limited capacity for self-renewal. J Neurosci. 2007; 27:14248–14259. [PubMed: 18160632]
28. Sousa VH, Miyoshi G, Hjerling-Leffler J, Karayannis T, Fishell G. Characterization of Nkx6-2-derived neocortical interneuron lineages. Cereb Cortex. 2009; 19(Suppl 1):i1–i10. [PubMed: 19363146]
29. Fletcher AL, Malhotra D, Acton SE, Lukacs-Kornek V, Bellemare-Pelletier A, Curry M, Armant M, Turley SJ. Reproducible isolation of lymph node stromal cells reveals site-dependent differences in fibroblastic reticular cells. Front Immunol. 2011; 2:35. [PubMed: 22566825]
30. Cupedo T, Vondenhoff MF, Heeregrave EJ, De Weerd AE, Jansen W, Jackson DG, Kraal G, Mebius RE. Presumptive lymph node organizers are differentially represented in developing mesenteric and peripheral nodes. J Immunol. 2004; 173:2968–2975. [PubMed: 15322155]
31. Vondenhoff MF, van de Pavert SA, Dillard ME, Greuter M, Goverse G, Oliver G, Mebius RE. Lymph sacs are not required for the initiation of lymph node formation. Development. 2009; 136:29–34. [PubMed: 19060331]
32. Krautler NJ, Kana V, Kranich J, Tian Y, Perera D, Lemm D, Schwarz P, Armulik A, Browning JL, Tallquist M, et al. Follicular dendritic cells emerge from ubiquitous perivascular precursors. Cell. 2012; 150:194–206. [PubMed: 22770220]
33. Tronche F, Kellendonk C, Kretz O, Gass P, Anlag K, Orban PC, Bock R, Klein R, Schütz G. Disruption of the glucocorticoid receptor gene in the nervous system results in reduced anxiety. Nat Genet. 1999; 23:99–103. [PubMed: 10471508]
34. Chang JE, Turley SJ. Stromal infrastructure of the lymph node and coordination of immunity. Trends Immunol. 2015; 36:30–39. [PubMed: 25499856]
35. Koning JJ, Mebius RE. Interdependence of stromal and immune cells for lymph node function. Trends Immunol. 2012; 33:264–270. [PubMed: 22153930]

36. Chai Q, Onder L, Scandella E, Gil-Cruz C, Perez-Shibayama C, Cupovic J, Danuser R, Sparwasser T, Luther SA, Thiel V, et al. Maturation of lymph node fibroblastic reticular cells from myofibroblastic precursors is critical for antiviral immunity. Immunity. 2013; 38:1013–1024. [PubMed: 23623380]

37. Cupedo T, Jansen W, Kraal G, Mebius RE. Induction of secondary and tertiary lymphoid structures in the skin. Immunity. 2004; 21:655–667. [PubMed: 15539152]

38. Mizoguchi T, Pinho S, Ahmed J, Kunisaki Y, Hanoun M, Mendelson A, Ono N, Kronenberg HM, Frenette PS. Osterix marks distinct waves of primitive and definitive stromal progenitors during bone marrow development. Dev Cell. 2014; 29:340–349. [PubMed: 24823377]

39. Ono N, Ono W, Mizoguchi T, Nagasawa T, Frenette PS, Kronenberg HM. Vasculature-associated cells expressing nestin in developing bones encompass early cells in the osteoblast and endothelial lineage. Dev Cell. 2014; 29:330–339. [PubMed: 24823376]

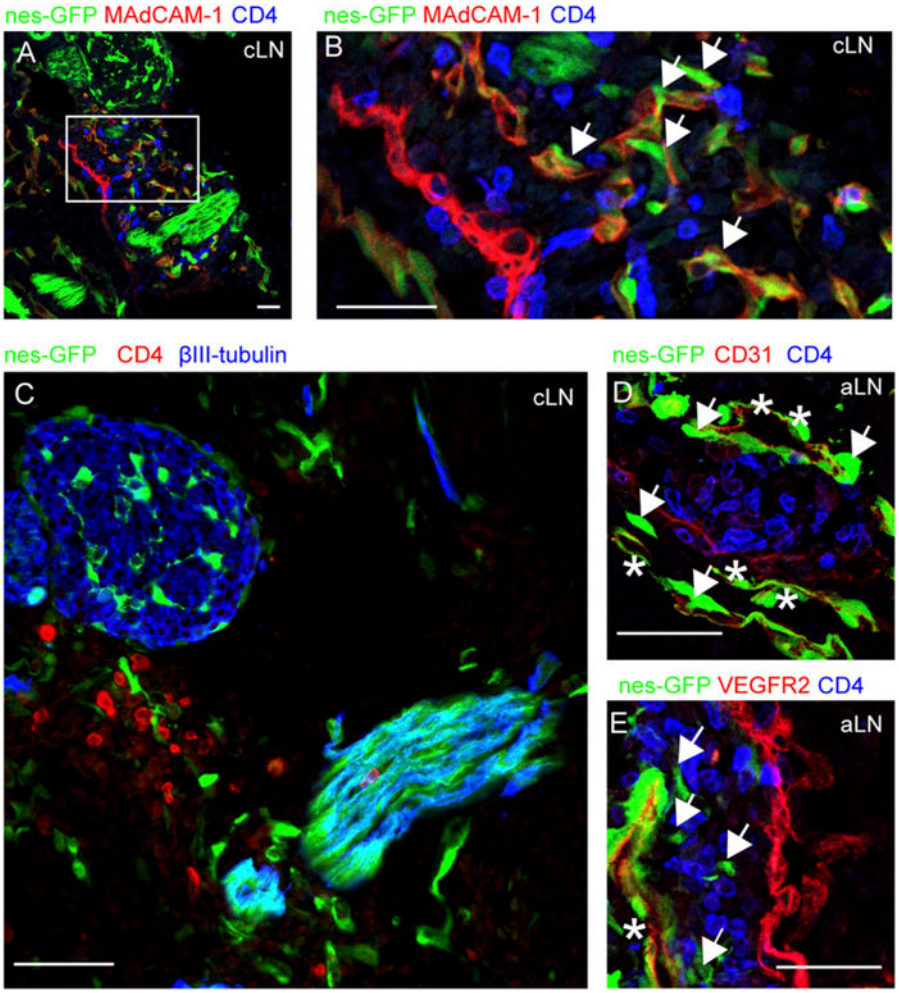

FIGURE 1.

Nestin-expressing stromal cells are present in E14.5 developing lymph nodes. (**A**–**E**) Immunofluorescence microscopy of lymph node anlagen of E14.5 nes-GFP mice. (A and B) Primitive lymph nodes were identified by CD4 (in blue), MAdCAM-1 (in red), and nestin-GFP cells (in green). (B) Magnification of a cervical lymph node anlage, containing MAdCAM-1^{+}nestin-GFP^{+} cells (indicated with an arrow). (C) Cervical lymph node anlage found in close vicinity to bright GFP-expressing structures that coexpressed βIII-tubulin (in blue). (D and E) Axillary lymph nodes containing nestin-GFP cells that were either positive (asterisk) or negative (arrows) for CD31 (D, red) or VEGFR2 (E, red). Scale bars, 25 μm. Data are representative of four individual nestin-GFP embryos. aLN, axillary lymph node; cLN, cervical lymph node.

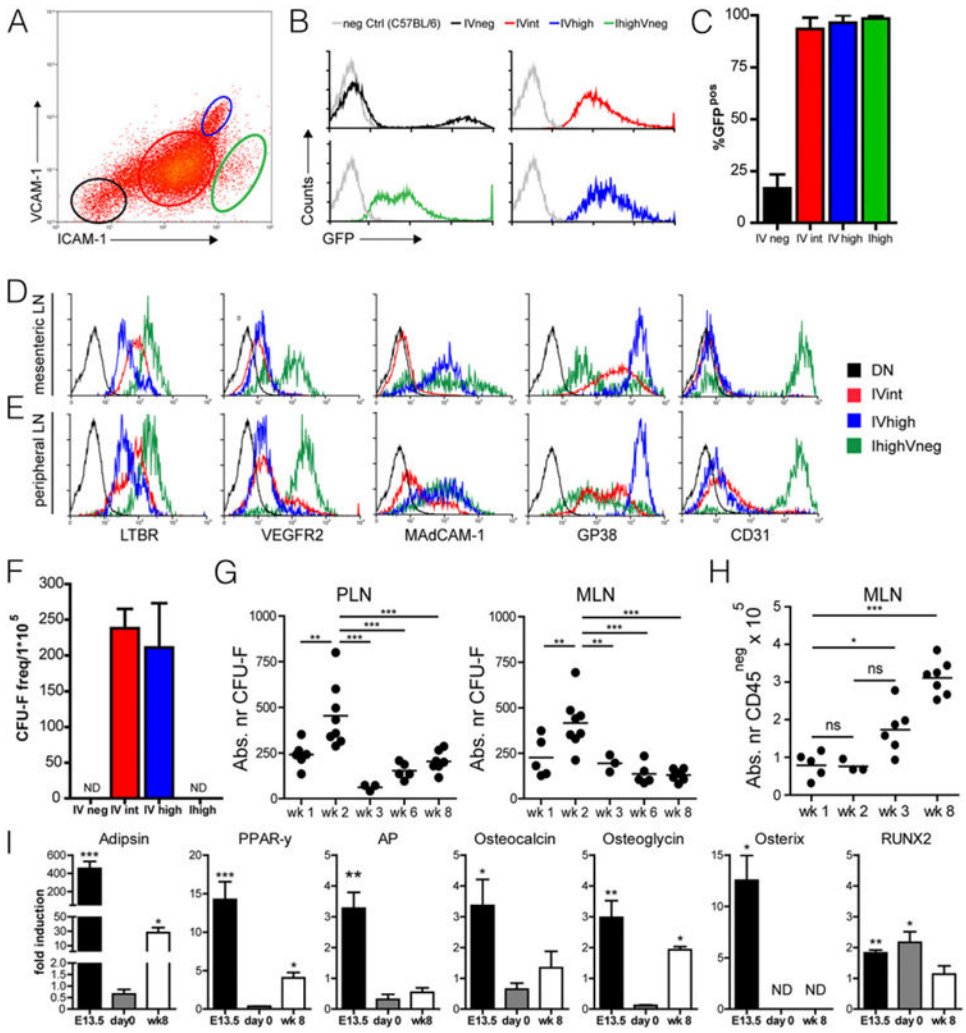

FIGURE 2.

Nestin expression marks lymphoid tissue organizer cells. (**A**–**C**) GFP expression by CD45^{-}ICAM-1^{-}VCAM-1^{-}(IV^{-}, black), CD45^{-}ICAM-1^{int}VCAM-1^{int} (IV^{int}, red), CD45^{-}ICAM-1^{high}VCAM-1^{high} (IV^{high}, blue), and CD45^{-}ICAM-1^{high}VCAM-1^{int} (I^{high}, green) cells derived from day 0 mesenteric lymph node single-cell suspensions from nestin-GFP mice. (C) Quantification of GFP expression by IV^{-}, IV^{int}, IV^{high}, and I^{high} cells derived from day 0 mesenteric lymph node single-cell suspensions from nestin-GFP mice ($n = 2$ individual experiments, at least five animals per group; data are represented as mean ± SEM). (**D** and **E**) FACS analysis of IV^{-}, IV^{int}, IV^{high}, and I^{high} stromal cells within day 0 mesenteric and peripheral lymph nodes. (D and E) One representative example out of three individual experiments with at least five animals per group. (**F**) CFU fibroblast capacity of sorted populations of IV^{-}, IV^{int}, IV^{high}, and I^{high} cells derived from single-cell suspensions of day 0 mesenteric lymph nodes ($n = 2$ individual experiments, at least five animals per group; data are represented as mean ± SEM). (**G** and **H**) Absolute numbers of CFU fibroblast capacity in both peripheral and mesenteric lymph nodes (G) and absolute numbers of CD45^{-} stromal cells in mesenteric lymph nodes (H) at various time points after birth. Each dot represents a set of lymph nodes obtained from a single mouse ($n \geq 3$; ANOVA; $^{**}p$

< 0.01, ***$p < 0.001$, data are represented as mean). (**I**) Quantative RT-PCR of genes associated with adipogenic (adipsin and peroxisome proliferator-activated receptor γ2 [PPAR-y]) and osteogenic (alkaline phosphatase [AP]), osteocalcin, osteoglycin, osterix, and RUNX2) differentiation of cultured mesenchymal precursors at day 0 and week 8 after birth. E13.5 precursor cells served as positive control. Data are represented as mean ± SEM, $n \geq 2$, unpaired two-tailed *t* test. *$p < 0.05$, **$p < 0.01$ ***$p < 0.001$. nd, not detected.

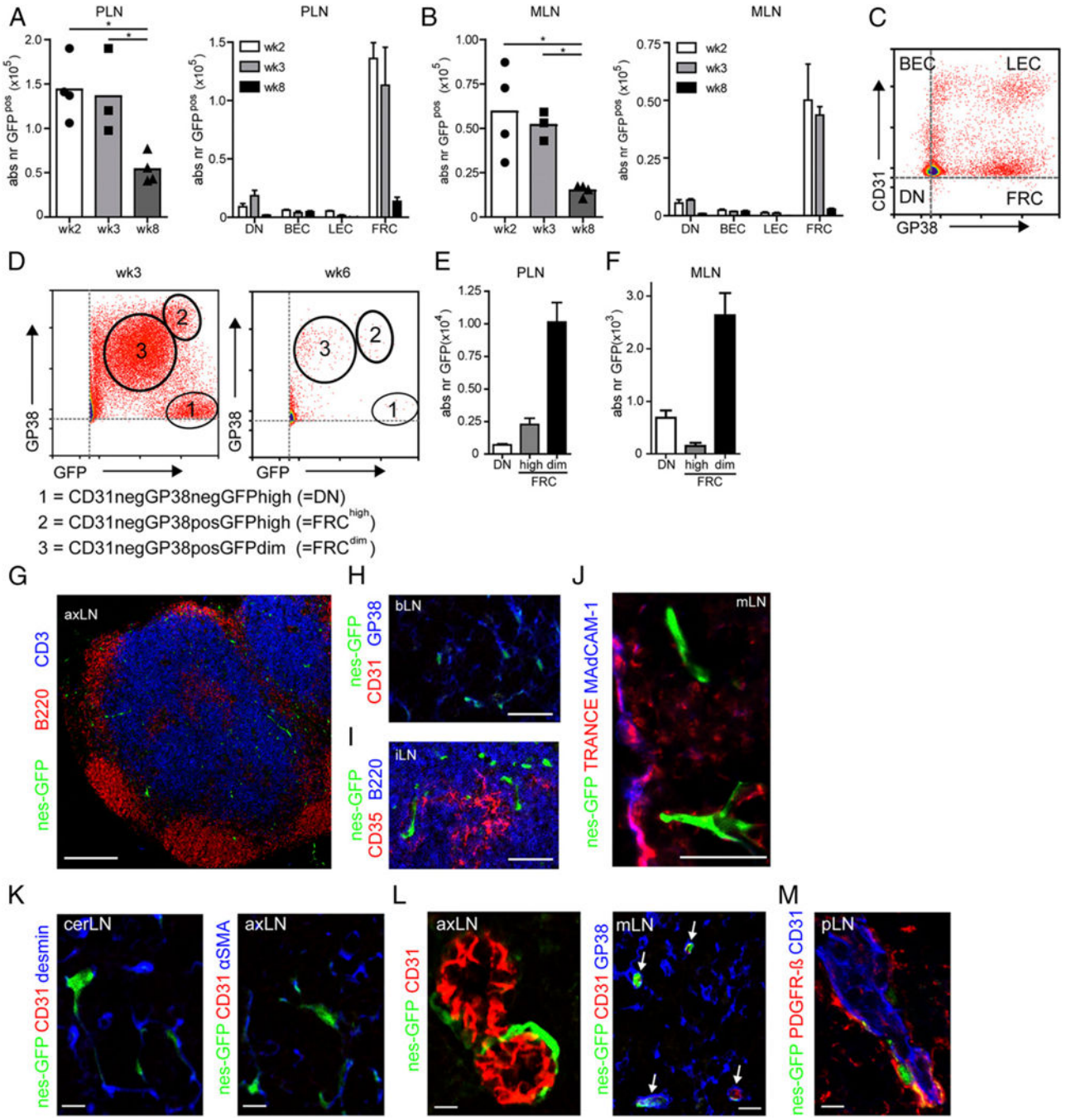

FIGURE 3.

Postnatal nestin expression decreases over time and remains present in adult lymph nodes. (**A**–**C**) Absolute number of nestin-GFP^{+} cells as well as their distribution over the four major stromal subsets (C) in peripheral and mesenteric lymph nodes. (**D**) FACS analysis showing distinct nestin^{+} cells based on GFP and gp38 expression in week 3 and week 6 nestin-GFP mice with 1) CD31^{-}gp38^{-}GFP^{high} (DN), 2) CD31^{-}gp38^{+}GFP^{high} (FRC^{high}), and 3) CD31^{-}gp38^{+}GFP^{dim} (FRC^{dim}) cells. (**E** and **F**) Absolute numbers of DN, FRC^{high}, and FRC^{dim} cells in adult nestin-GFP mice (week 8) in PLN (E) and MLN (F). Data are

represented as mean ± SEM, $n = 3$ or more, ANOVAwith Bonferroni posttest: $*p < 0.05$). (**G**–**M**) Immunofluorescence analysis of lymph nodes derived from adult nestin-GFP mice. (G) Distribution of nestin-GFP$^+$ mesenchymal precursors (green) in adult lymph nodes taken from 12-wk-old nestin-GFP mouse, stained for B cells (B220; red) and T cells (CD3; blue). (H–J) Higher magnification of a T cell area in which gp38$^+$ (blue) stromal cells and nestin-GFP$^+$ cells (green) are present (H), nestin-GFP$^+$ cells (green) in B cell area stained for FDCs (CD35; red) and B cells (B220; blue) (I), and nestin-GFP$^+$ (green) cells in subcapsular sinus area together with TRANCE (red) as well as MAdCAM-1 (blue) (J). (K) Immunofluorescence images of the T cell area of lymph nodes where nestin-GFP$^+$ cells (green) express desmin (blue, left panel) and α-SMA (blue, right panel). (L) Nestin-GFP$^+$ cells (green) around CD31$^+$ HEVs (red). (M) Nestin-GFP$^+$ cells (green) around CD31$^+$ HEVs (blue) stained for PDGFR-β (red). Images are representative for both peripheral and mesenteric lymph nodes of three individual animals. Scale bars, 250 (G), 10 (J–M), and 50 μm (H and I). axLN, axillary lymph node; cerLN, cervical lymph node; iLN, inguinal lymph node; mLN, mesenteric lymph node.

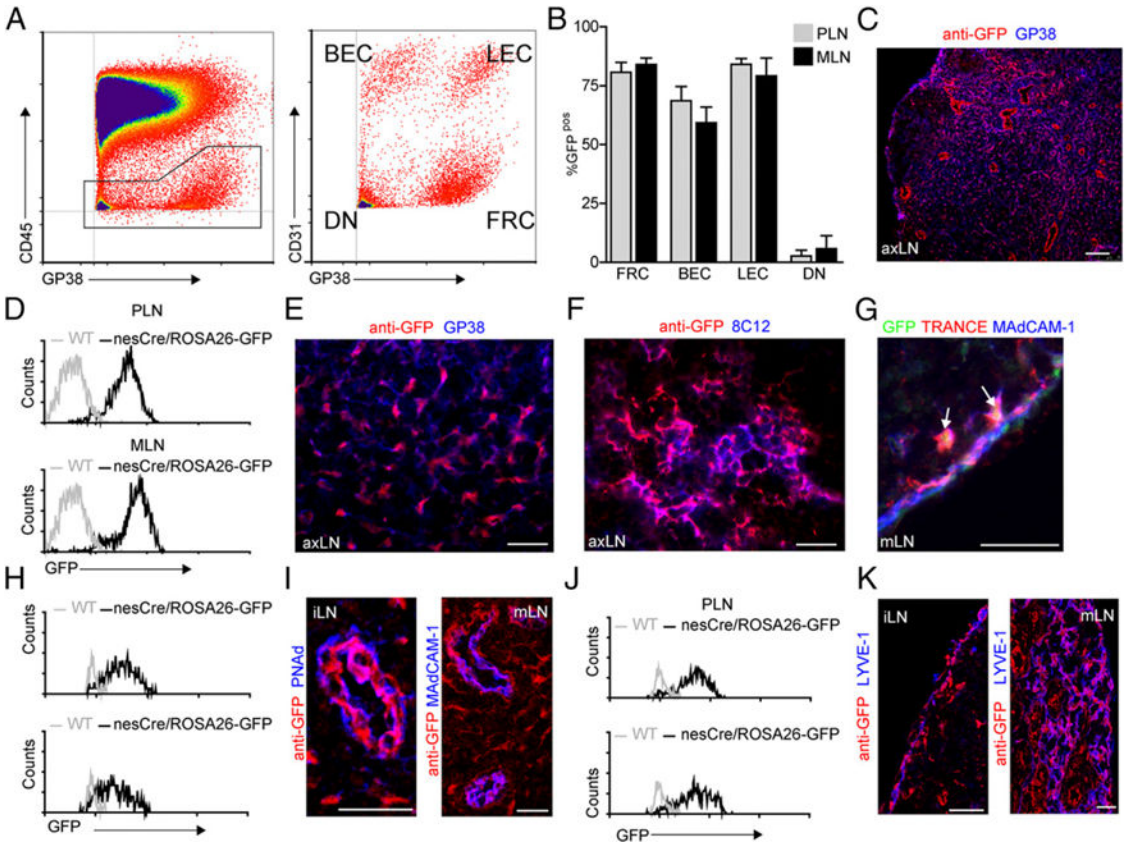

FIGURE 4.

Nestin precursors give rise to the major subsets of endothelial- and mesenchymal-derived lymph node stromal cells. (**A**) Representative FACS analysis example of single-cell suspensions of peripheral and mesenteric lymph nodes derived from nestin-cre/ROSA26-GFP mice stained for CD45, gp38, and CD31 to identify the four stromal cell populations (FRCs, gp38^{+}CD31^{-}; LECs, gp38^{+}CD31^{+}; BECs, gp38^{-}CD31^{+}; DN, gp38^{-}CD31^{-}). (**B**) Percentage GFP^{+} stromal cells within peripheral or mesenteric lymph nodes of nestin-cre/ROSA26-GFP mice (n = 4 [age 12–14 wk]; data are represented as mean ± SEM). (**C**) Immunofluorescene analysis showing the distribution of GFP expression identified by anti-GFP staining (in red) of a peripheral lymph node derived from adult nestin-cre/ROSA26-GFP. Scale bar, 75 μm. (**D**, **H**, and **J**) Histograms showing the expression of GFP within the FRC population (D), BEC population (H), and LEC population (J) of adult nestin-cre/ROSA26-GFP (black line) peripheral and mesenteric lymph nodes. (**E**–**G**, **I**, and **K**) Immunofluorescence images of lymph nodes from nestin-cre/ROSA26-GFP stained with anti-GFP (in red) and in blue gp38 (E), 8C12 (F). (G) In the subcapsular sinus, endogenous GFP expression (in green) could be identified, and arrowheads indicate cells that stain positive for TRANCE (in red) and MAdCAM-1 (in blue). Subsequent sections were stained with anti-GFP (in red) and PNAd or MAdCAM-1 (in blue) to identify HEVs (I) and Lyve-1 (in blue) to identify LECs (K). Images are representative for both peripheral and mesenteric lymph nodes of four individual animals, 12–14 wk of age. Scale bars, 75 (C), 50 (E–G), and 25 μm (I and K). axLN, axillary lymph node; iLN, inguinal lymph node; mLN, mesenteric lymph node.

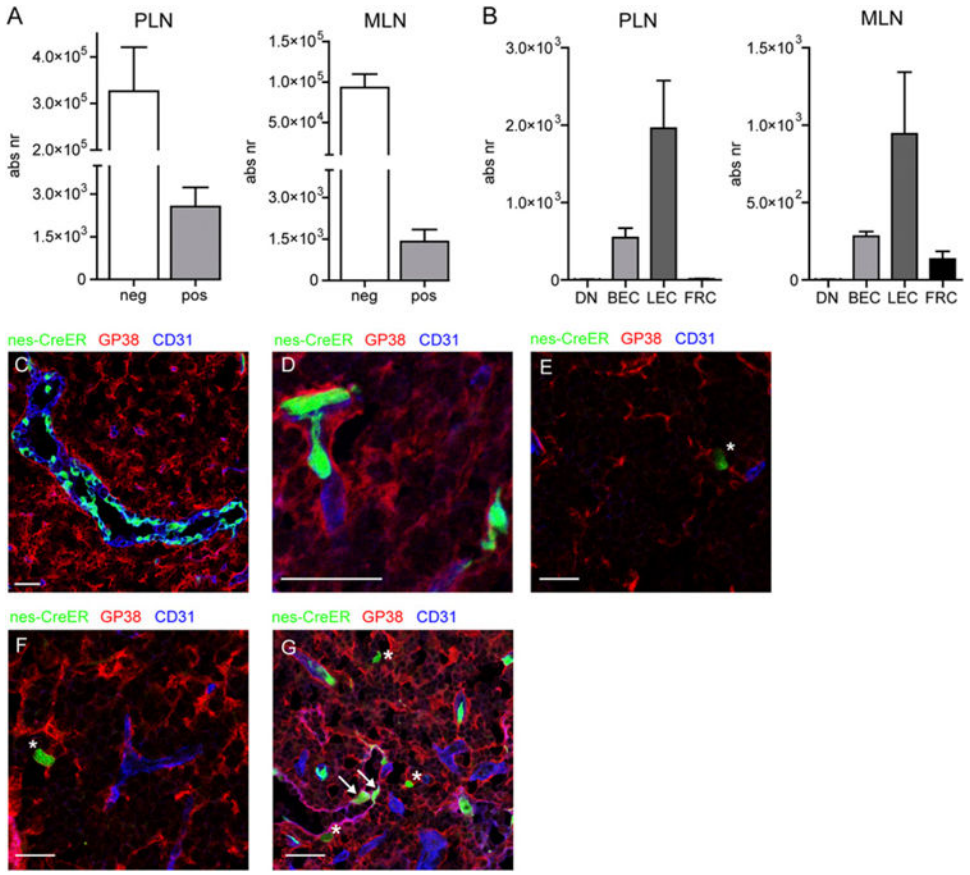

FIGURE 5.

During later stages of lymph node development, nestin predominantly labels endothelial cells. (**A**) Graphs showing the absolute number of GFP^- and GFP^+ cells of nes-creER c ROSA26-GFP mice that received tamoxifen at day 17 after birth and were analyzed 4 wk later. (**B**) Graphs showing the distribution of GFP^+ cells among the various lymph node stromal populations. (**C–G**) Immunofluorescence analysis of nes-creER × ROSA26-GFP mice that received tamoxifen at p17 and were analyzed 4 wk later. (C–F) Lymph node sections stained for gp38 (red) and CD31 (blue) showing GFP^+ HEVs (C), GFP^+ capillaries (D), GFP^+ $gp38^+CD31^-$ stromal cells (indicated with asterisks, E–G), and GFP^+gp38^+ $CD31^+$ lymphatic endothelial cells (indicated with arrows, G). Images are representative of lymph nodes of five individual animals (A and B) or three individual mice (C–G). Scale bars, 25 μm.

Table I

List of primer sequences used for RT-PCR

Primer	Sequence (5′→3′)
Adipsin Fw	TGCATCAACTCAGAGTGTCAATCA
Adipsin Rv	TGCGCAGATTGCAGGTTGT
Alkaline phospathase Fw	CACAATATCAAGGATATCGACGTGA
Alkaline phospathase Rv	ACATCAGTTCTGTTCTTCGGGTACA
β-actin Fw	TGACAGGATGCAGAAGGAGATTACT
β-actin Rv	AGCCACCGATCCACACAGA
Cyclo Fw	ACCCATCAAACCATTCCTTCTGTA
Cyclo Rv	TGAGGAAAATATGGAACCCAAAGA
HPRT Fw	CCTAAGATGAGCGCAAGTTGAA
HPRT Rv	CCACAGGACTAGAACACCTGCTAA
Osteocalcin Fw	GGGCAATAAGGTAGTGAACAG
Osteocalcin Rv	GCAGCACAGGTCCTAAATAGT
Osteoglycin Fw	ACCATAACGACCTGGAATCTGT
Osteoglycin Rv	AACGAGTGTCATTAGCCTTGC
Osterix Fw	ATGGCGTCCTCTCTGCTTGA
Osterix Rv	GAAGGGTGGGTAGTCATTTG
PPAR-y Fw	GCCTTGCTGTGGGGATGTCTC
PPAR-y Rv	GGAGATCTCCGCCAACAGCTT
RUNX-2 Fw	GTGACAGTGGACGGTCCCC
RUNX-2 Rv	TCATCAAGCTTCTGTCTGTGCC
Ubiquitin Fw	AGCCCAGTGTTACCACCAAG
Ubiquitin Rv	ACCCAAGAACAAGCACAAGG

Cyclo, cyclophillin; Fw, forward; HPRT, hypoxanthine phosphoribosyltransferase; PPAR-y, peroxisome proliferator-activated receptor γ2; Rv, reverse.